UNIVERSITY of GLASGOW

Department of Physics & Astronomy
Experimental Particle Physics Group
Kelvin Building, University of Glasgow,
Glasgow, G12 8QQ, Scotland
Telephone: +44 (0)141 339 8855 Fax: +44 (0)141 330 5881

GLAS-PPE/2005-17
30th November 2005

Measurement of the Electron Structure Function at LEP energies.

B. Muryn[1], T. Szumlak[2],

[1] AGH - University of Science and Technology, Cracow, Poland
[2] University of Glasgow, Glasgow, G12 8QQ, Scotland

Abstract

The hadronic part of the Electron Structure Function (ESF) has been measured for the first time, using e^+e^- data collected by the DELPHI experiment at LEP, at electron scattering energy from $\sqrt{s} = 91.18 - 209.5$ GeV. The data analysis is simpler than that of the measurement of the photon structure function. The ESF data are compared to predictions of phenomenological models based on the photon structure function. The GRVLO and SAS parameterisations do not seem to reproduce the data at high virtualities of the probing photons. It is shown that the quasi-real photon virtuality contribution is significant. The presented data can serve as a cross-check of the photon structure function analyses and help in refining existing parametrisations.

HEP2005 International Europhysics Conference on High Energy Physics
21-27 Jul 2005 Lisboa, Portugal

1 Introduction

Single tag $e^+e^- \mapsto e^\pm X$ collisions can be used to determine both the photon [1] and electron [2, 3] hadronic structure functions. The photon has been studied both theoretically and experimentally for many years [1, 4, 5]. Experimental results on the electron structure function (ESF) are presented for the first time in this paper. Although both analyses start

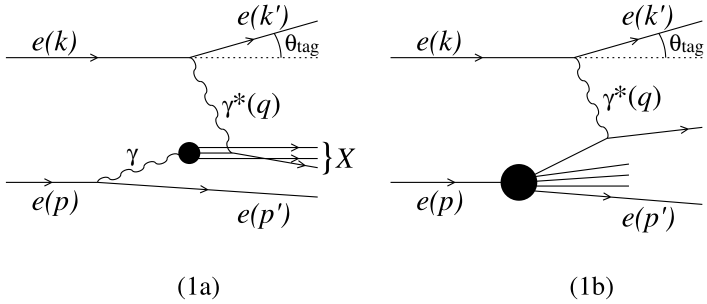

Figure 1: Deep inelastic scattering on a photon target (1a), and on an electron target (1b); p, p', k and k' denote the corresponding four-momenta and q is the four-momentum of the radiated photon.

from the same set of events the procedures are quite different mainly due to different kinematics. In the photon case (Fig. 1a) the spectrum of virtual photons emitted by the (untagged) electron is strongly peaked at small virtualities P^2 (this quantity can be expressed in terms of the untagged electron four-momenta, $P^2 = -(p-p')^2$), approximating the photon to be real.However, non-zero virtuality plays a role [3]. In the electron case (Fig. 1b) the photon scatters on a real particle so the problem does not appear. Another difference is the determination of the Bjorken variables x (z) representing the fraction of the struck parton momentum with respect to the photon (electron). In the first case, since the photon momentum is not known, the total hadronic mass W must be used to determine x,

$$x \cong \frac{Q^2}{Q^2+W^2}\ , \tag{1}$$

where $Q^2 = -(k-k')^2$ is the negative momentum squared of the deeply virtual (probing) photon. The z variable for the electron is determined simply - as in the classical deep inelastic scattering i.e. from the scattered electron variables only (see below). A certain drawback of the electron structure function is its expected shape: it contains the sharply peaked photon distribution and is dominated by this shape. Hence the data can be reanalyzed in terms of the electron structure function and the results compared to the usual photon structure function analysis. We also expect that the data on both the electron and photon structure functions will help to improve phenomenological parametrisations of the quark content inside the photon and the electron.

The case of the electron structure function is illustrated in Fig. 1b. The upper (tagged) electron emits a photon of high virtuality $Q^2 = -q^2$ and scatters off the target electron constituents. The cross-section for such a process under the assumption that $Q^2 \gg P^2$, is:

$$\frac{d^2\sigma_{ee\to eX}}{dzdQ^2} = \frac{2\pi\alpha^2}{zQ^4}\left[\left(1+(1-y)^2\right)F_2^e(z,Q^2) - y^2F_L^e(z,Q^2)\right], \tag{2}$$

where

$$y = 1-(E_{\rm tag}/E)\cos^2(\theta_{\rm tag}/2), \tag{3}$$

with E, $E_{\rm tag}$ and $\theta_{\rm tag}$ being the beam electron initial, final energy and scattering angle, respectively. $F_2^e(z,Q^2)$ and $F_L^e(z,Q^2)$ are the electron structure functions related to the transversal and longitudinal polarization states of the target photon. The parton momentum fraction, z, is defined in the standard (deep inelastic) way:

$$z = \frac{Q^2}{2pq} = \frac{\sin^2(\theta_{\rm tag}/2)}{E/E_{\rm tag} - \cos^2(\theta_{\rm tag}/2)}\ , \tag{4}$$

and is measured, by means of the tagged electron variables only. The virtuality of the probing photon can be also expressed in terms of E_{tag}, θ_{tag} as follows:

$$Q^2 = 4EE_{tag}\sin^2(\theta_{tag}/2). \tag{5}$$

The structure function $F_2^e(z,Q^2)$, which dominates the cross-section at small y, has a simple partonic interpretation:

$$F_2^e(z,Q^2) = z\sum_{i=q,\bar{q}} e_i^2 f_i^e(z,Q^2), \tag{6}$$

where e_i and f_i^e are the i-th quark/anti-quark fractional charge and density. In e^+e^- experiments the two-photon hadronic cross-section is expressed in terms of two real photon structure functions $F_2^\gamma(x,Q^2)$ and $F_L^\gamma(x,Q^2)$ which leads to the formula analogous to (2)

$$\frac{d^2\sigma_{e\gamma\to eX}}{dxdQ^2} = \frac{4\pi\alpha^2}{xQ^4}\left[(1+(1-y_\gamma)^2)F_2^\gamma(x,Q^2) - y_\gamma^2 F_L^\gamma(x,Q^2)\right], \tag{7}$$

where y_γ is the photon energy with respect to the electron energy, F_2^γ and F_L^γ are the photon structure functions related to the transverse and longitudinal target photon polarization states respectively. Since the photon structure function analysis makes use of the same $\sigma_{ee\to eX}$ cross-section, as stated in equation (2), in order to extract the $\sigma_{e\gamma\to eX}$ cross-section must be corrected by a density of photons in the target electron $f_\gamma^e(y_\gamma,P^2)$ (photon flux). In general the photon flux depends on momentum transfer squared, P^2, taken at the target photon vertex:

$$f_\gamma^e(y_\gamma,P^2) = \frac{\alpha}{2\pi P^2}\left[\frac{1+(1-y_\gamma^2)}{y_\gamma} - 2y_\gamma\frac{m_e^2}{P^2}\right], \tag{8}$$

where α is the fine structure constant and m_e is the electron mass. The flux is an unmeasurable for single tag events. It is customary to replace the above formula by a real photon flux function. This approximation may not be correct since the anti-tag condition results in the existence of off-shell photons with virtualities $P^2 \le P^2_{max}$, where P^2_{max} is the maximum value of four-momentum transfer in the lower vertex and it is fixed by the STIC luminometer geometry (see section 2.1) and antitag condition. This problem is eliminated in the case of the electron structure function.

In [2, 3] the construction of the electron structure function has been presented together with the Q^2 evolution equations and their asymptotic solutions. This approach has also been compared with the "photon structure function" approach. Although the determination of the electron and photon structure functions is quite different the functions are simply interrelated:

$$F_2^e(z,Q^2,P^2_{\max}) = \int_z^1 dy_\gamma \int_{P^2_{\min}}^{P^2_{\max}} dP^2 f_\gamma^e(y_\gamma,P^2)\, F_2^\gamma(z/y_\gamma,Q^2,P^2), \tag{9}$$

where $P^2_{\min} = m_e^2 y_\gamma^2/(1-y_\gamma)$. The above formula enables any existing parametrisation of the photon structure function, both real ($P^2=0$) and virtual (integrated over P^2), to be tested on the measured electron structure function.

In this paper we report on the measurement of the electron structure function using LEPI and LEPII data. Section 2 describes the selection process of the event sample collected for the analysis and the detector efficiency determination. Section 3 contains the most important details concerning the ESF evaluation. In Section 4 we present conclusions from the measurement.

2 Experimental procedure

2.1 The DELPHI detector

A detailed description of the DELPHI detector and former references can be found in [6] and therefore only short account of the subdetectors relevant to presented analysis is discussed. The DELPHI detector provide 3-dimensional information about curvature and energy deposition with very good spatial resolution as well as identification of leptons and hadrons over most of the solid angle.

The most important parts of the setup for the ESF analysis could be divided into two groups. First one consists of the detectors which provide reconstruction of the hadronic final state. In general the detectors could be identified as DELPHI tracking subsystem containing: the Inner Detector, the Time Projection Chamber (the main DELPHI tracking device) and the Outer Detector. Those devices are operated in the 1.23 T magnetic field parallel to the beam axis. Tracking in the forwar (backward) regions is provided by the Forward Chambers. The tracking detectors cover polar angles from 20 - 160 degrees (with reciprocal overlap) at radii 120 to 2600 mm for barrel region. The Forward Chambers cover polar angles from 11 to 35 degrees (forward sector) and 147 to 169 degrees (backward sector). Using these subsystem the momentum resolution is $\frac{\sigma(p)}{p} = 0.0015\cdot p$, where p is momentum in GeV. In order to determine the hadronic final state Hadron Calorimeter must be also used.

The second group consists of detectors providing the electromagnetic shower energy measurement. Among them the crucial one is the luminosity calorimeter STIC (Small Angle Tile Calorimeter). The STIC is lead-scintillator calorimeter formed by two cylindrical detectors placed on both sides of the DELPHI interaction point at a distance of 2200 mm and covers angular region between 29 and 185 mrad in polar angle at radii 65 to 420 mm. The STIC energy measurements are used to asure the tag condition.

subsectionEvent Selection The analysis has been carried out with the data samples collected by DELPHI at both LEPI and LEPII centre-of-mass energies ranging from 92.5 GeV up to 209.5 GeV and corresponding to integrated luminosities of 72 pb^{-1} at LEPI and 487 pb^{-1} at LEPII. The most important criterion to select $\gamma\gamma$ events was that one of the two scattered electrons [1)] Examination of the e^+e^- annihilation processes generated by PYTHIA (version 6.142) [7] and those corresponding to four-fermion events produced with EXCALIBUR [8] proved that the major background contributions originate from Z^0 hadronic decays and the two-photon production of $\tau\tau$ pairs. In order to suppress these the following cuts were imposed:

- The vector sum of the transverse momenta of all charged particles, normalised to the total beam energy had to be greater than 0.12 for LEPI (0.14 for LEPII data taking).
- The normalised (like above) sum of the absolute values of the longitudinal momenta of all charged particles (including tagged electron) had to be greater than 0.6.
- The angle between the transverse momenta of the tagged electron and of the charged particles system had to be greater than 120°.
- The maximum of the visible invariant mass was 40 GeV for LEPI (60 GeV for LEPII data taking).

Among the 21430 events of the LEPI data set (101913 for LEPII) with one high-energy deposit in the STIC calorimeter, 2168 events (9697 for LEPII) passed the above criteria. The total background contribution estimated from the simulation amounted to 111 events for LEPI (1027 for LEPII).

3 Determination of the Electron Structure Function

The ESF can be extracted as a function of two variables z and Q^2 from formula (2) under assumption that the longitudinal term F_L^e is negligible and reads

$$F_2^e(\xi,Q^2) = C\frac{Q^4}{(1+(1-y)^2)}\frac{d^2\sigma_{ee\to eX}}{d\xi dQ^2}\ , \qquad (10)$$

where $\xi = log_{10}(z)$ and C is the product of all constant factors.

The measured function $F_2^e(\xi,Q^2)$ was corrected in each $\Delta\xi_i\Delta Q_k^2$ bin by the corresponding detector response function $E(\xi,Q^2)$, yielding the reconstructed ESF $F_2^e(\xi,Q^2)$. Then the Electron Structure Function is averaged over Q^2 in the considered region of the probing photon virtuality leaving only the ξ dependence. The ESF is shown in Figs. 2 and 3 for five Q^2 intervals, $Q^2 \in (4.5,15)\,\mathrm{GeV}^2$, $Q^2 \in (16,20)\,\mathrm{GeV}^2$, $Q^2 \in (20,30)\,\mathrm{GeV}^2$, $Q^2 \in (30,50)\,\mathrm{GeV}^2$ and $Q^2 \in (50,80)\,\mathrm{GeV}^2$.

Since, according to formula 5, the lower kinematical limit of Q^2 depends on the cut on the minimum $\theta_{tag} = 2.5°$ angle of the tagged electron (fixed by the STIC detector) and its energy, the $Q^2 \in (4.5,15)\,\mathrm{GeV}^2$ ESF distribution in Fig. 2 corresponds to LEPI and Fig. 3 to LEPII data.

Such a procedure is justified since the migration effect of events generated in any of the (ξ,Q^2) bins to neighbouring bins, after passing the detector simulation, is small.

4 Conlusions

The hadronic part of the electron structure function has been measured and has been found to agree with the predictions based on the photon structure function. The proposed method is explicit and simpler than the photon structure analysis as it does not use the unfolding procedure. It allows the virtuality of the probed photon to be taken into account correctly. It is shown that the migration of events between z-bins (electron) is much smaller than between x-bins (photon). The statistical uncertainties are well understood since in each bin of the measured ESF they reflect a Poisson error whereas statistical uncertainties obtained from the unfolding procedure for the photon analysis have never been discussed.

All the presented models follow the data within one standard deviation up to $Q^2 \in (50,80)\,\mathrm{GeV}^2$. For higher virtualities of the probing photons, a tiny excess of events at small values of z and a reduction of events at the higher ones are observed (see Fig. 3d). A fit to the experimental points hints to such a possible trend. Similar tendency for the Photon Structure Function depending on the x scaling variable is also seen in data of ALEPH ($<Q^2>= 67\,\mathrm{GeV}^2$) [**?**] and OPAL ($<Q^2>= 767\,\mathrm{GeV}^2$) [**?**]. It should be stressed that the inclusion of the photon virtuality is important - the difference between the two SaS parametrisations (P^2-dependent and $P^2 = 0$) are of the same order as between SaS and GRVLO (both with $P^2 = 0$).

[1)] electron is used for both electron and positron.

References

[1] E. Witten, Nucl. Phys. **B120**, 189 (1977);
C.H. Llewellyn-Smith, Phys. Lett. **79B**, 83 (1978);
R.J. DeWitt et al., Phys. Rev. **D19**, 2046 (1979);
T.F. Walsh and P. Zerwas, Phys. Lett. **36B**, 195 (1973);
R.L. Kingsley, Nucl. Phys. **B 60**, 45 (1973).

[2] W. Słomiński and J. Szwed, Phys. Lett. **B387**, 861 (1996);
Acta Phys. Polon. **B27** 1887 (1996); ibid **B28** 1493 (1997);
W. Słomiński and J. Szwed, Eur. Phys. J. **C22**, 123 (2001);

[3] W. Słomiński, Acta Phys. Polon. **B30**, 369 (1999).

[4] H.J. Behrend et al., CELLO Collaboration, Phys. Lett. **126B**, 391 (1983);
Ch. Berger et al., PLUTO Collaboration, Phys. Lett. **142B**, 111 (1984);
W. Bartel et al., JADE Collaboration, Zeit. f. Phys. **C24**, 231 (1984);
M. Althoff et al., TASSO Collaboration, Zeit. f. Phys. **C31**, 527 (1986);
H. Aihara et al., TPC/2γ Collaboration, Zeit. f. Phys. **C34**, 1 (1987);

[5] T. Sasaki et al., AMY Collaboration, Phys. Lett. **252B**, 491 (1990);
R. Akers et al., OPAL Collaboration, Zeit. f. Phys. **C61**, 199 (1994);
S.K. Sahu et al., AMY Collaboration, Phys. Lett. **B346**, 208 (1995);
P. Abreu et al., DELPHI Collaboration, Zeit. f. Phys. **C69**,223 (1996);
K. Ackerstaff et al., OPAL Collaboration, Zeit. f. Phys. **C74**, 33 (1997);
M. Acciarri et al., L3 Collaboration, Phys. Lett. **B436**, 403 (1998);
ibid. **B447**, 147 (1999; ALEPH Collaboration, Phys. Lett.**B458**, 152 (1999).

[6] DELPHI Collab., P.Aarnio et al., Nucl. Instr. and Methods., **A378**, 57 (1996)

[7] http://www.thep.lu.se/˜torbjorn

[8] http://charlton.home.cern.ch/charlton/excalibur/excalibur.html

[9] M. Gluck, E. Reya, A. Vogt, Dynamical parton distributions revisited,
Eur.Phys.J. C5, (1998)

[10] G. A. Schuler, T. Sjostrand, Parton distributions of the virtual photon,
Phys.Lett. B376, (1996);
G. A. Schuler, T. Sjostrand, **Z.Phys.Rev. D50** (1994)

[11] S. Nova, A. Olshevsky, T. Todorov, DELPHI-90-35 (unpublished).

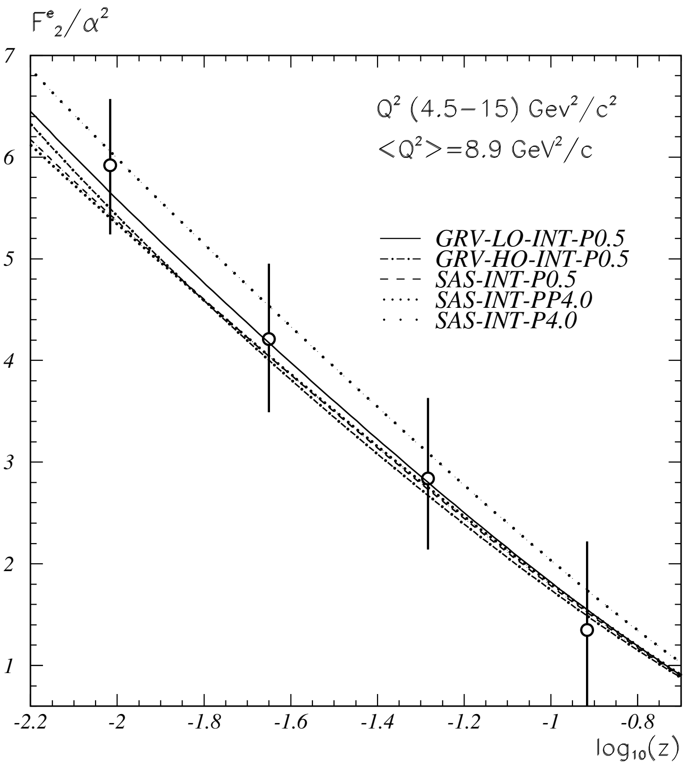

Figure 2: LEPI data. The electron structure function measured for $Q^2 \in (4.5, 15)\,\mathrm{GeV}^2$.

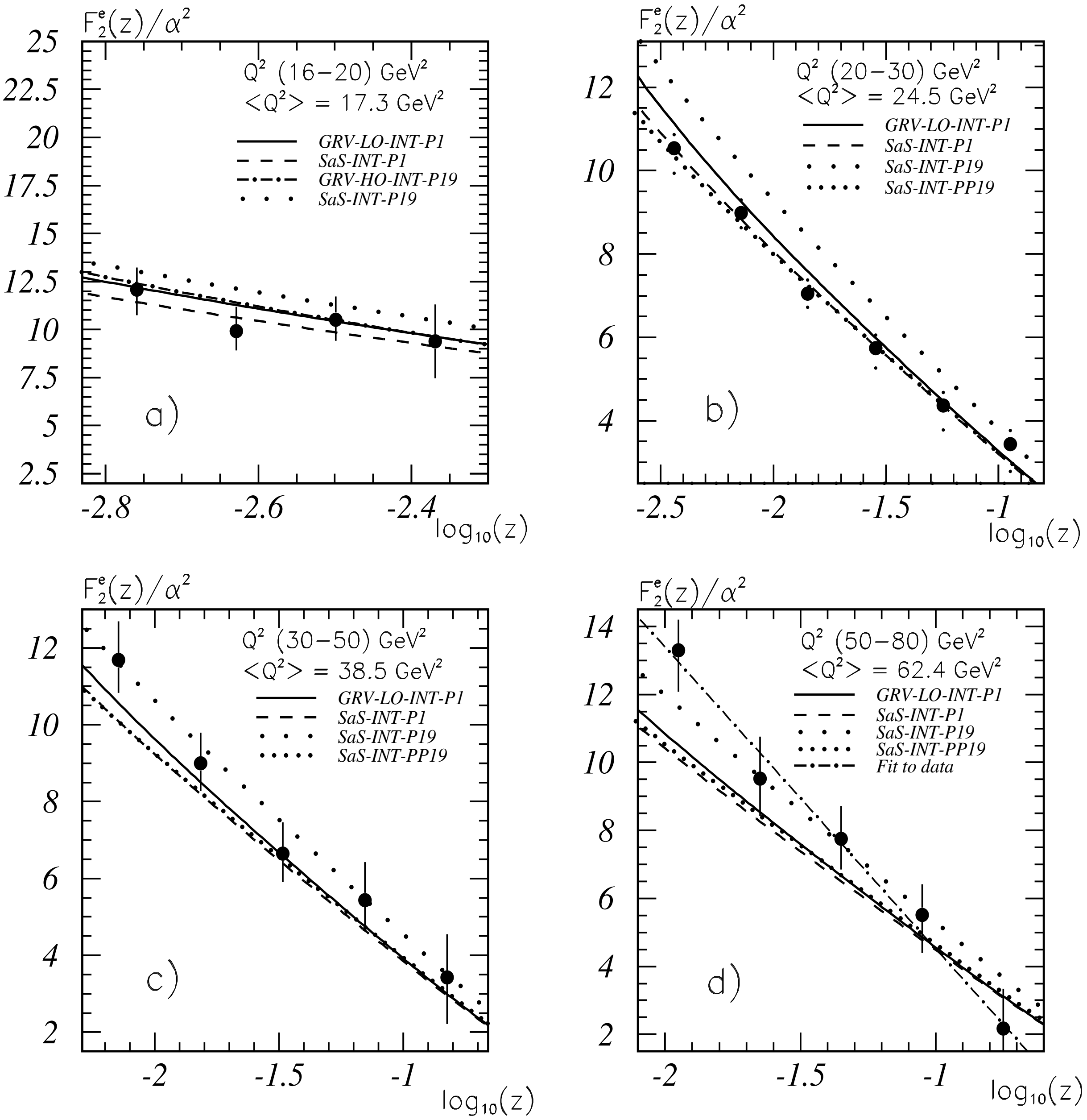

Figure 3: LEPII data.The electron structure function measured for (a) $Q^2 \in (16,20)\,\mathrm{GeV}^2$, (b) $Q^2 \in (20,30)\,\mathrm{GeV}^2$, (c) $Q^2 \in (30,50)\,\mathrm{GeV}^2$, (d) $Q^2 \in (50,80)\,\mathrm{GeV}^2$.